Electronic Supplementary Information

Reverse synthesis of star anise-like cobalt doped Cu-MOF/$Cu_{2+1}O$ hybrid materials based on $Cu(OH)_2$ precursor for high performance supercapacitors

Xueying Cao[a], Liang Cui[b]*, Bingping Liu[c], Ying Liu[a], Dedong Jia[a]*, Wenrong Yang[d], Joselito M. Razal[d], Jingquan Liu[a,b]*

[a]College of Material Science and Engineering, Institute for Graphene Applied Technology Innovation, Qingdao University, Qingdao, 266071, Shandong, China.

[b]College of Material Science and Engineering, Linyi University, Linyi, 276000 Shandong, China.

[c]College of Chemistry and Pharmaceutical Sciences, Qingdao Agricultural University, Qingdao 266071, Shandong, China.

[d]School of Life and Environmental Sciences, Institute for Frontier Materials, Deakin University, Geelong, VIC 3216, Australia.

*Corresponding author

E-mail: clzkzy@163.com; jliu@qdu.edu.cn; jiadedong@qdu.edu.cn;

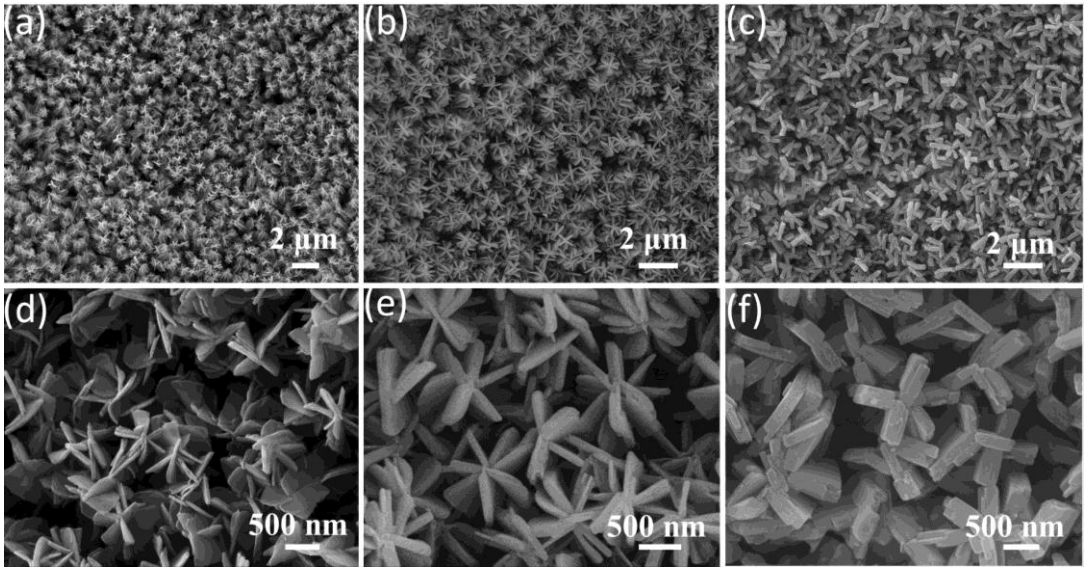

Fig. S1. SEM images of (a, d) 0.05Co/Cu-MOF/$Cu_{2+1}O$, (b, e) 0.2Co/Cu-MOF/$Cu_{2+1}O$ and (c, f) 0.3Co/Cu-MOF/$Cu_{2+1}O$.

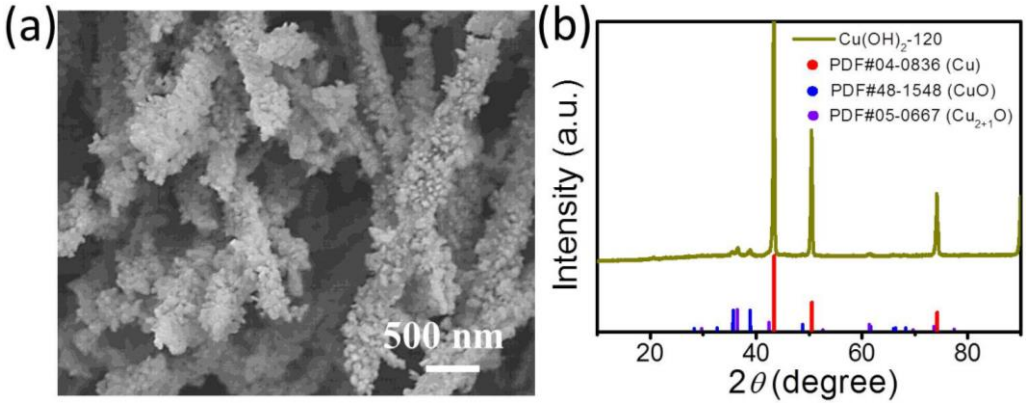

Fig. S2. (a) SEM image and (b) XRD pattern of $Cu(OH)_2$-120.

The $Cu(OH)_2$-120 sample was prepared to explore the growth mechanism of $Cu_{2+1}O$ in Cu-MOF/$Cu_{2+1}O$ composite. Fig. S2a shows the $Cu(OH)_2$-120 has a morphology of nanorods encapsulated with nano-particles. As shown in Fig. S2b, after solvothermal reaction in DMF, $Cu(OH)_2$ was transformed into a mixture of CuO and $Cu_{2+1}O$, but both the CuO and $Cu_{2+1}O$ reveal weak peaks, which confirms the trace contents of them. Compared with Fig. 3a in revised manusicript, the weaker peaks of $Cu_{2+1}O$ shown in Fig. S2b confirm that the Cu-MOF may act as a mediator to guide the growth of $Cu_{2+1}O$ and there should be a synergistic effect between

Cu-MOF and $Cu_{2+1}O$ in the growth process of $Cu_{2+1}O$.

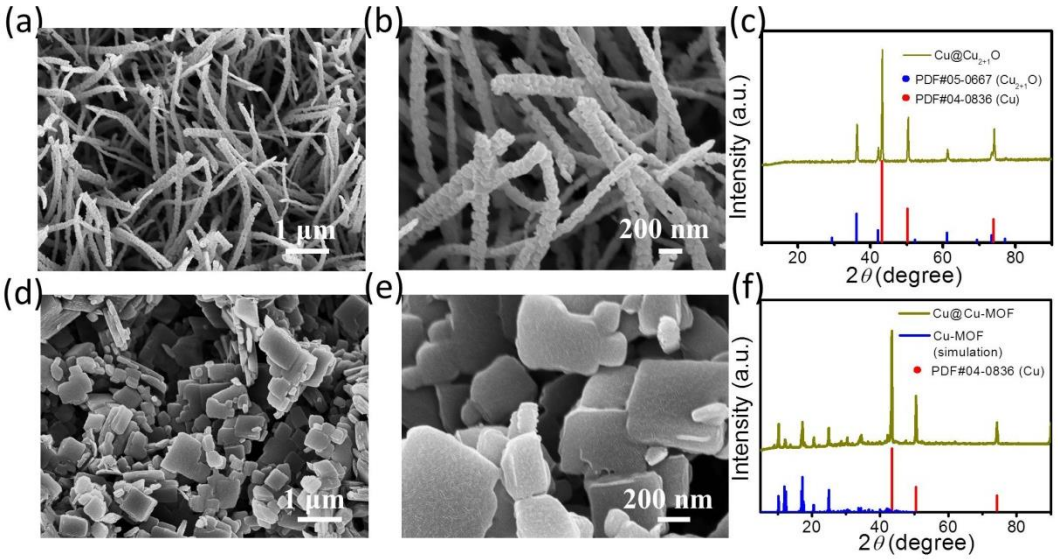

Fig. S3. (a, b) SEM images and (c) XRD pattern of $Cu@Cu_{2+1}O$, (d, e) SEM images and (f) XRD pattern of Cu@Cu-MOF.

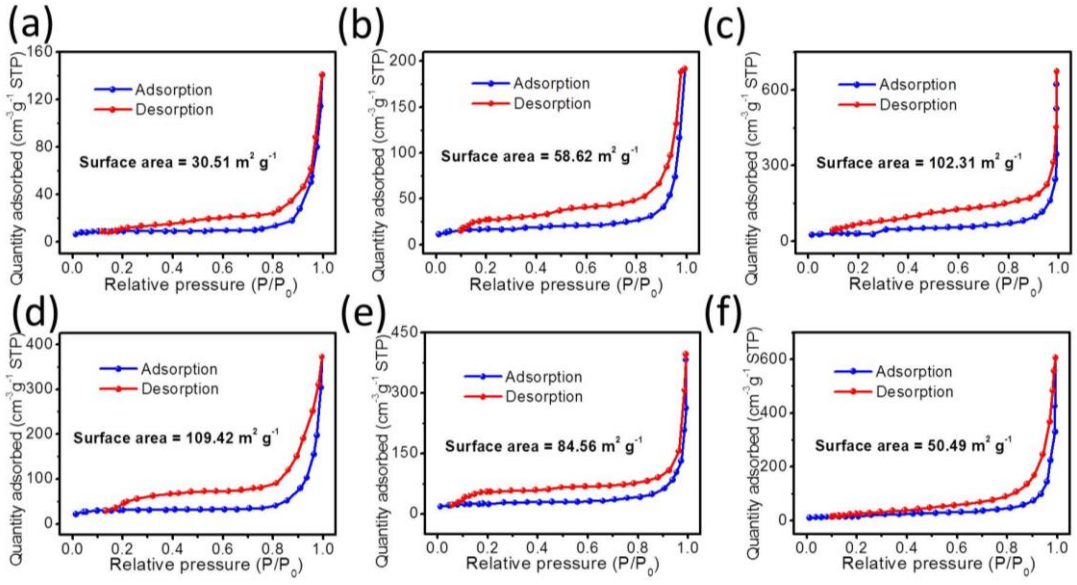

Fig. S4. N_2 adsorption-desorption isotherms of (a) $Cu(OH)_2$, (b) Cu-MOF/$Cu_{2+1}O$, (c) 0.05Co/Cu-MOF/$Cu_{2+1}O$, (d) 0.1Co/Cu-MOF/$Cu_{2+1}O$, (e) 0.2Co/Cu-MOF/$Cu_{2+1}O$ and (f) 0.3Co/Cu-MOF/$Cu_{2+1}O$.

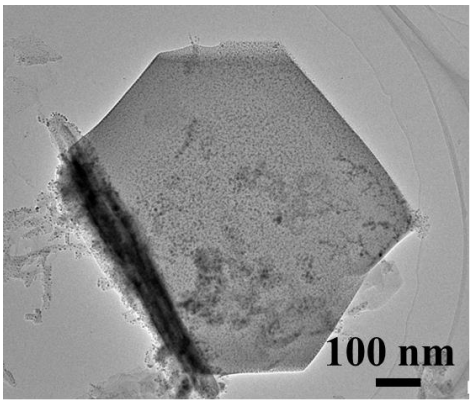

Fig. S5. TEM image of 0.1Co/Cu-MOF/$Cu_{2+1}O$ after electron beam damage.

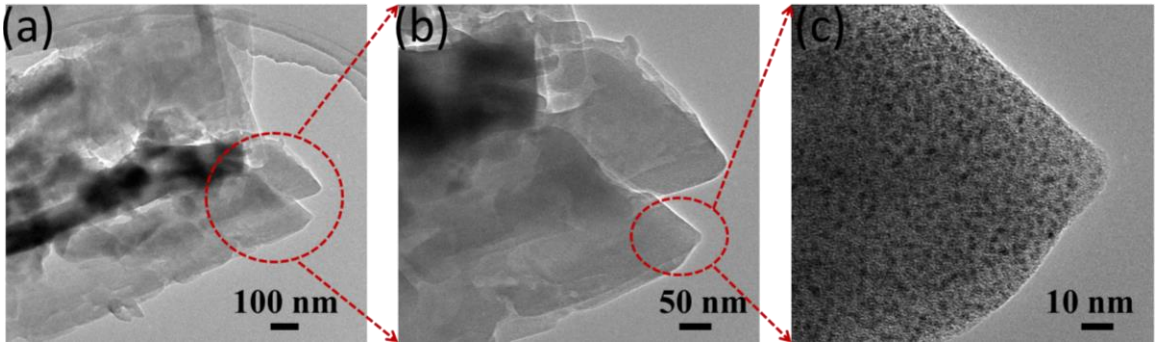

Fig. S6. TEM images of 0.1Co/Cu-MOF/$Cu_{2+1}O$ at different magnifications.

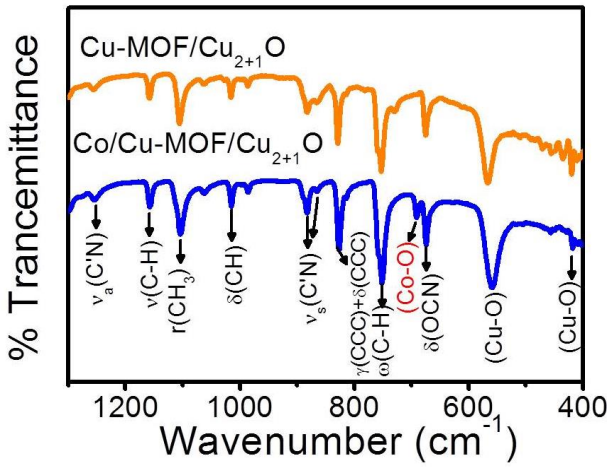

Fig. S7. The fingerprint area of FTIR spectra for Cu-MOF/$Cu_{2+1}O$ and Co/Cu-MOF/$Cu_{2+1}O$ samples.

Fig. S7 shows the fingerprint area of FTIR spectra for Cu-MOF/$Cu_{2+1}O$ and Co/Cu-MOF/$Cu_{2+1}O$ samples. The bands at 673, 1063, 1104 and 1257 cm^{-1}, should be ascribed to the residual DMF in samples and can be identified as δ(OCN), δ(CH), r(CH_3) and ν_a(C'N), respectively.[1] Meanwhile, the bands at 755, 826, 882 and 1148 cm^{-1} are related to the ω(C-H), γ(CCC) + δ(CCC), ν_s(C'N) and ν(C-H) from Cu-MOF, respectively.[2] The bands observed at 416 and 568 cm^{-1} are related to the vibrational modes of Cu-O phase.[3] The new band at ~680 cm^{-1} in Co/Cu-MOF/$Cu_{2+1}O$ should belong to the ν(Co-O) mode,[4] which further proves the successful doping of cobalt.

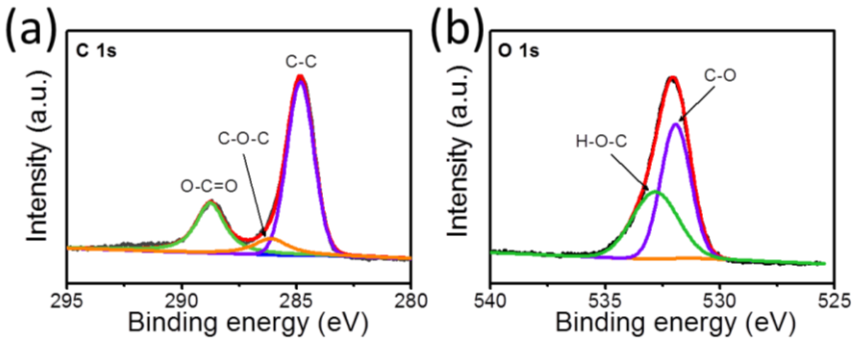

Fig. S8. High-resolution XPS spectra for (a) C 1s and (b) O 1s of 0.1Co/Cu-MOF/$Cu_{2+1}O$.

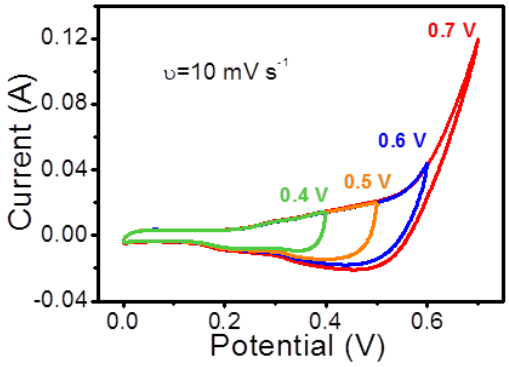

Fig. S9. CV curves of 0.1Co/Cu-MOF/$Cu_{2+1}O$ in different potential windows at a scan rate of 10 mV s^{-1}. (0 to 0.5 V is the optimal potential window while the polarization phenomenon appeared when the potential range was enlarged.)

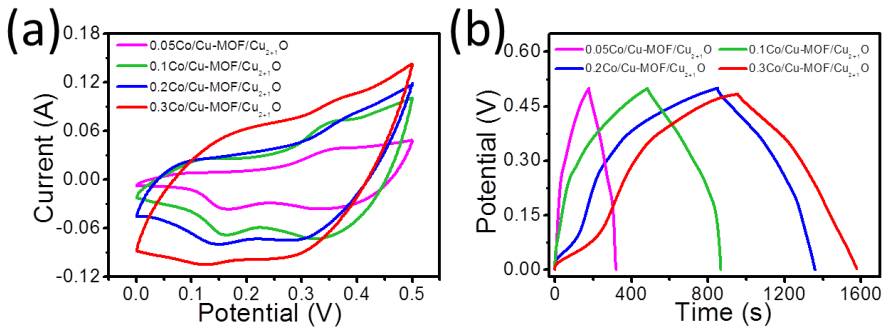

Fig. S10. (a) CV curves of 0.05Co/Cu-MOF/$Cu_{2+1}O$, 0.1Co/Cu-MOF/$Cu_{2+1}O$, 0.2Co/Cu-MOF/$Cu_{2+1}O$ and 0.3Co/Cu-MOF/$Cu_{2+1}O$ electrodes at a scan rate of 50 mV s^{-1}. (b) GCD curves of 0.05Co/Cu-MOF/$Cu_{2+1}O$, 0.1Co/Cu-MOF/$Cu_{2+1}O$, 0.2Co/Cu-MOF/$Cu_{2+1}O$ and 0.3Co/Cu-MOF/$Cu_{2+1}O$ electrodes at a current density of 2 mA cm^{-2}.

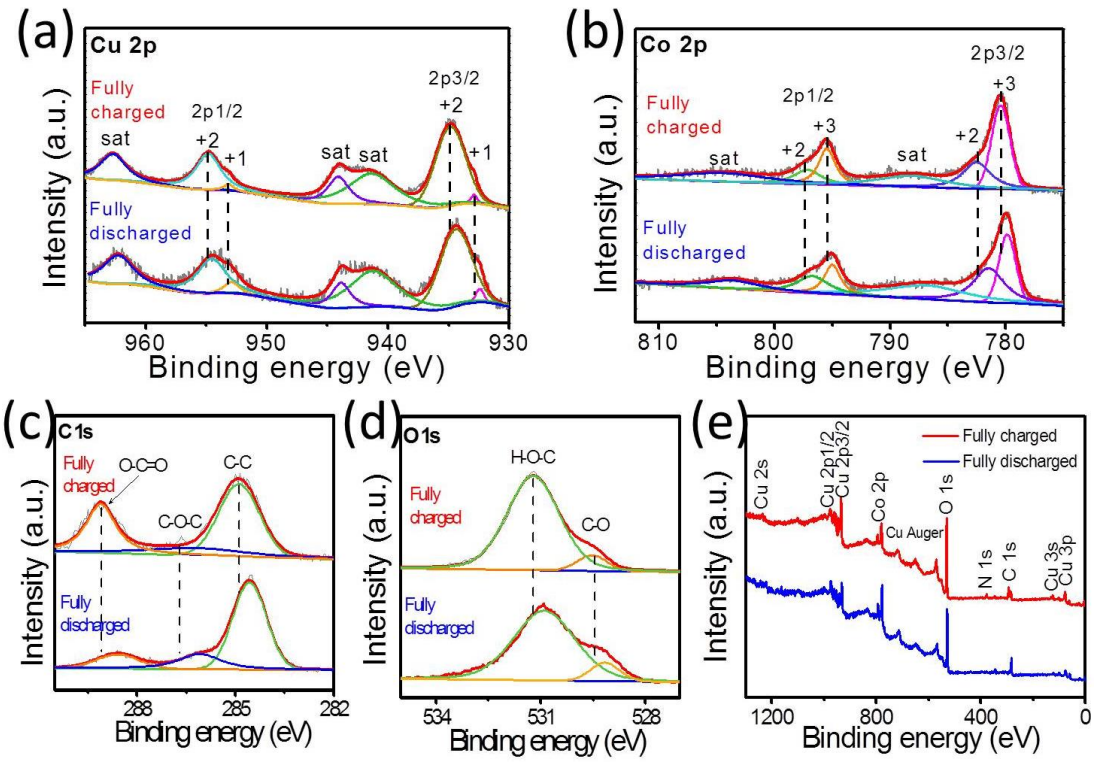

Fig. S11. High-resolution XPS spectra for (a) Cu 2p, (b) Co 2p, (c) C 1s and (d) O 1s of 0.1Co/Cu-MOF/$Cu_{2+1}O$ electrode and (e) XPS survey spectrum of 0.1Co/Cu-MOF/$Cu_{2+1}O$ electrode for fully charged and fully discharged states.

Fig. S11 shows the XPS spectra of the fully charged and discharged states of 0.1Co/Cu-MOF/$Cu_{2+1}O$ electrode. Compared with the XPS spectra of pristine 0.1Co/Cu-MOF/$Cu_{2+1}O$ electrode (Figs 3 and S8), there is none new peaks in Fig. S11. It is noteworthy that all of the peaks in Fig. S11a-d shift to a higher binding energy at fully charged state *versus* that at the fully discharged state, indicating the enhanced oxidation ability at fully charged state.[5] What's more, as shown in Fig. S11a, when the electrode was fully discharged from 0.5 V to 0 V, the peak intensities of Cu^{1+} 2p3/2 and Cu^{1+} 2p1/2 increased, which should be attributed to the reduction of Cu^{2+} to Cu^{1+}. Meanwhile, the peak intensities of Co^{2+} 2p3/2 and Co^{2+} 2p1/2 also increased as a result of reduction of Co^{3+} to Co^{2+} during discharge process (Fig. S11b). Since Co^{3+} and Co^{4+} ions have similar XPS spectra, Co^{4+} is likely to exist during charge discharge processes.[6]

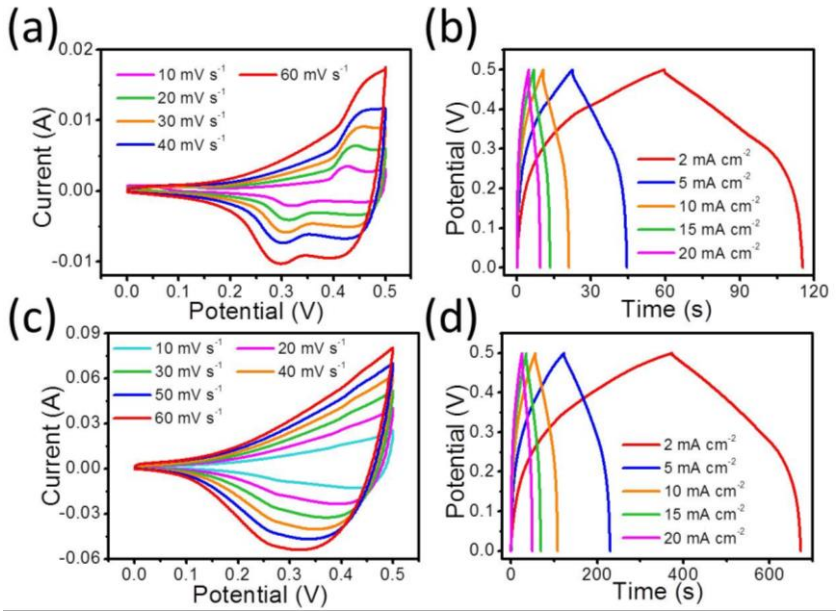

Fig. S12. (a) CV curves and (b) GCD curves of the $Cu(OH)_2$ electrode at various scan rates and different current densities. (c) CV curves and (d) GCD curves of the Cu-MOF/$Cu_{2+1}O$ electrode at various scan rates and different current densities.

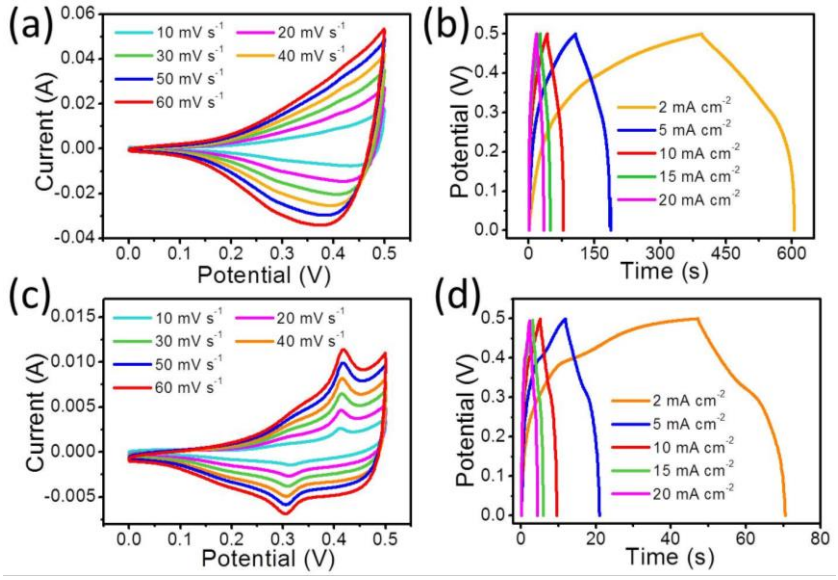

Fig. S13. (a) CV curves and (b) GCD curves of the Cu@$Cu_{2+1}O$ electrode at various scan rates and different current densities. (c) CV curves and (d) GCD curves of Cu@Cu-MOF electrode at various scan rates and different current densities.

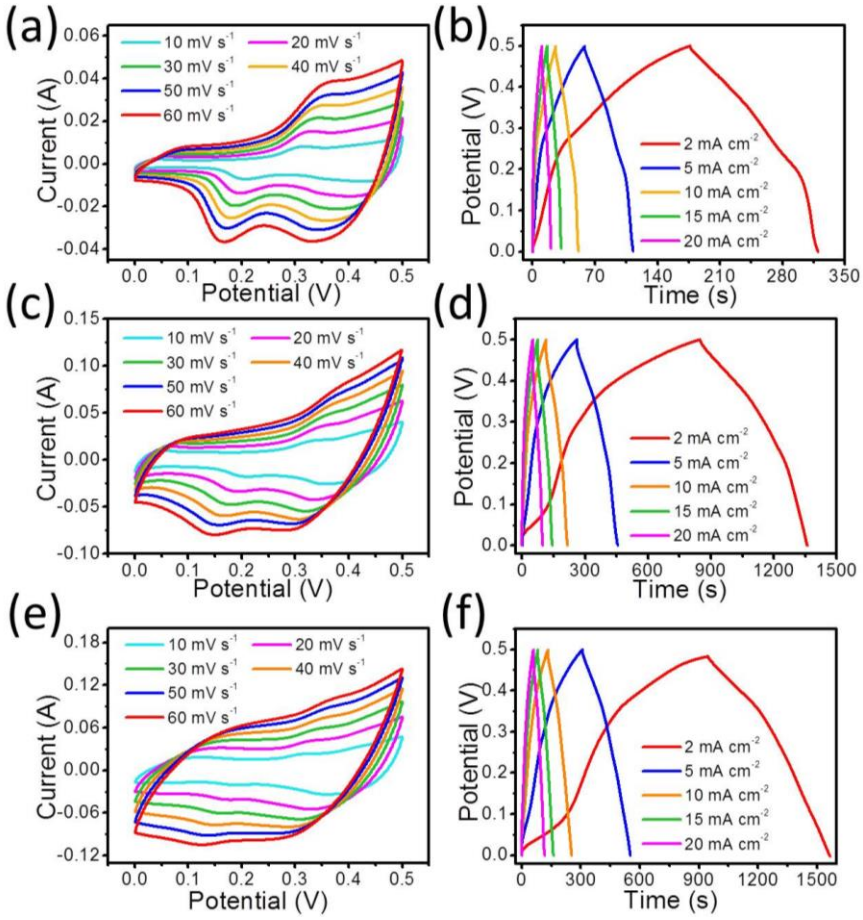

Fig. S14. (a) CV curves and (b) GCD curves of the 0.05Co/Cu-MOF/$Cu_{2+1}O$ electrode at various scan rates and different current densities. (c) CV curves and (d) GCD curves of the 0.2Co/Cu-MOF/$Cu_{2+1}O$ electrode at various scan rates and different current densities. (e) CV curves and (f) GCD curves of the 0.3Co/Cu-MOF/$Cu_{2+1}O$ electrode at various scan rates and different current densities.

Table S1. Comparison of the capacitance performance of our prepared electrodes with those of other previous reported MOF-based electrode materials.

Electrodes	Electrolyte	Rate	*C*m (F g^{-1})	Refs
0.05Co/Cu-MOF/$Cu_{2+1}O$	6 M KOH	1.33 A g^{-1}	389.30	This work
0.1Co/Cu-MOF/$Cu_{2+1}O$	6 M KOH	0.67 A g^{-1}	518.58	This work
0.2Co/Cu-MOF/$Cu_{2+1}O$	6 M KOH	0.40 A g^{-1}	412.60	This work
0.3Co/Cu-MOF/$Cu_{2+1}O$	6 M KOH	0.27 A g^{-1}	343.47	This work
Ni-based MOFs	6 M KOH	50 mV s^{-1}	125	[7]
ZIF-67	6 M KOH	200 mV s^{-1}	163	[8]
MOF-5	6 M KOH	5 A g^{-1}	220	[9]
Co-MOFs	2 M KOH	1 A g^{-1}	140	[10]
Fe-MIL-88B-NH_2	1 M KOH	2 A g^{-1}	95	[11]
ZIF-67	1 M KOH	2 A g^{-1}	188	[12]
ZIF-8	1 M $LiPF_6$	5 A g^{-1}	450	[13]
Co-based MOF	1 M LiOH	0.6 A g^{-1}	206	[14]
MnO_x-MHCF	1 M Na_2SO_4	5 mA cm^{-2}	127	[15]
Mn-BTC	0.5 M Na_2SO_4	1 A g^{-1}	374	[16]
IRMOF-3	1 M H_2SO_4	50 mV s^{-1}	190	[17]
Zn-MOFs	1 M H_2SO_4	1 A g^{-1}	477	[18]
MOF-74	1 M H_2SO_4	10 mV s^{-1}	193	[19]
ZIF-8	1 M H_2SO_4	5 A g^{-1}	200	[20]

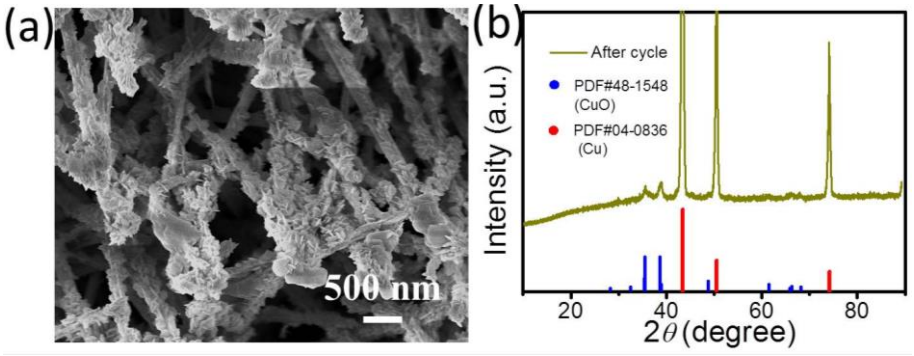

Fig. S15. (a) SEM image and (b) XRD pattern of 0.1Co/Cu-MOF/$Cu_{2+1}O$ after stability test for 5000 cycles.

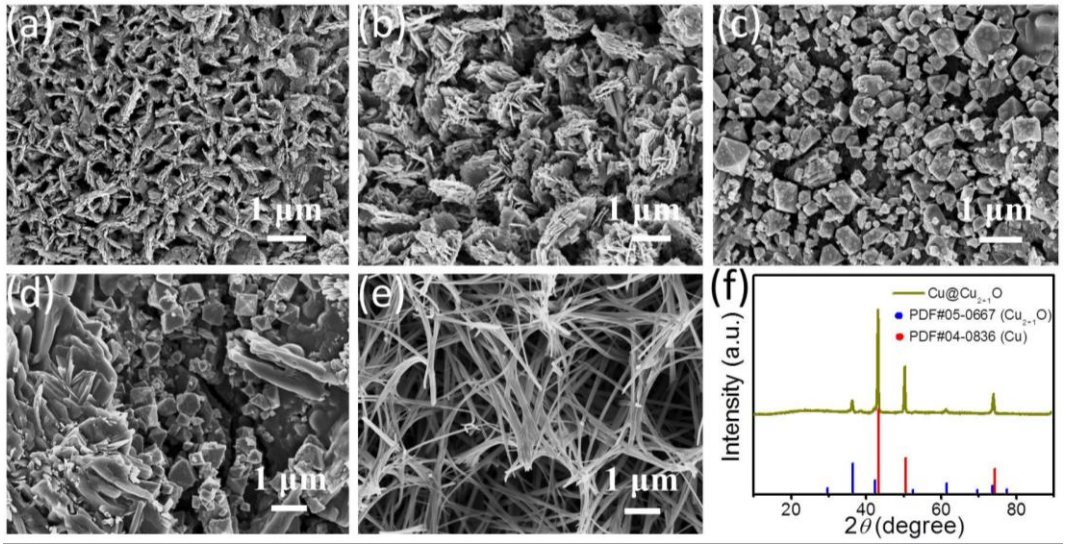

Fig. S16. The SEM images of 0.1Co/Cu-MOF/$Cu_{2+1}O$ sample incubated in a 6 M KOH solution without external voltage for (a) 1 day, (b) 2 days, (c) 3 days, (d) 4 days and (e) 5 days. (f) The XRD pattern of the 0.1Co/Cu-MOF/$Cu_{2+1}O$ sample after incubation for 5 days.

Fig. S16a-e show the morphological changes of 0.1Co/Cu-MOF/$Cu_{2+1}O$ sample incubated in a 6 M KOH solution without external voltage for one to five days respectively. From the SEM images, the nanorods assembled with nanosheets gradually dissolved to form stacked nanosheets at the first two days, which gradually dissolved the next two days and finally formed smooth nanowires array at the fifth day. Fig. S16f shows that the new nanowires array can be indexed to the $Cu_{2+1}O$ crystal structure (JCPDS no. 05-0667).

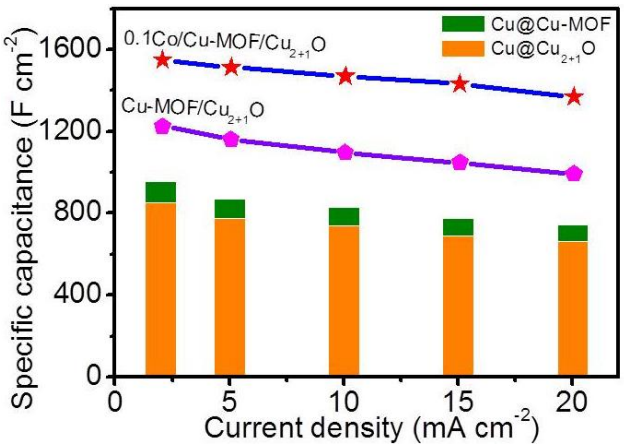

Fig. S17. The total capacitances of $Cu@Cu_{2+1}O$ and Cu-MOF electrodes compared with those of $0.1Co/Cu\text{-}MOF/Cu_{2+1}O$ and $Cu\text{-}MOF/Cu_{2+1}O$ electrodes at different current densities.

As shown in Fig. S17, both the capacitances of $0.1Co/Cu\text{-}MOF/Cu_{2+1}O$ and $Cu\text{-}MOF/Cu_{2+1}O$ electrodes are much larger than the total capacitances of $Cu@Cu_{2+1}O$ and Cu@Cu-MOF electrodes at different current densities, which confirms the synergistic effect on the electrochemical performance between Cu-MOF and $Cu_{2+1}O$ in our prepared $Cu\text{-}MOF/Cu_{2+1}O$ composite.

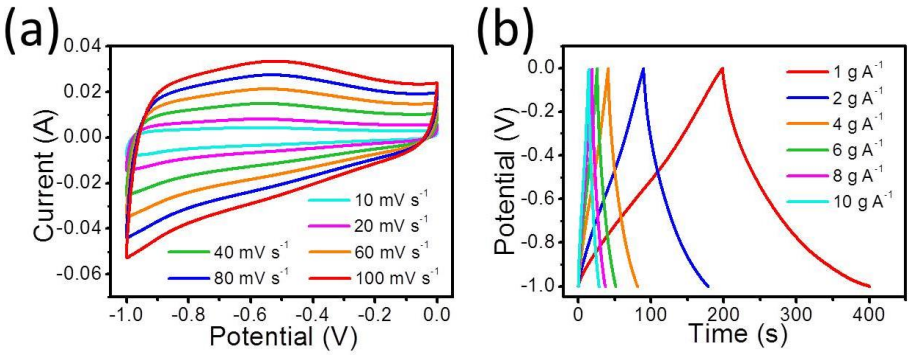

Fig. S18. (a) CV curves and (b) GCD curves of the AC electrode at various scan rates and different current densities.

1. K. Nishi, H. Komori, M. Kikuchi, N. Uehara, N. Fukunaga, K. Matsumoto, H. Watanabe, K. Nakajou, S. Misumi, A. Suenaga, *Eur. J. Inorg. Chem.,* 2010, **2009,** 2338-2343.

2. H. Embrechts, M. Kriesten, K. Hoffmann, W. Peukert, M. Hartmann, M. Distaso, *J. Phys. Chem. C,* 2018, **122,** 12267-12278.

3. B. Balamurugan, B. R. Mehta, *Thin Solid Films,* 2001, **396,** 90-96.

4. B. Pejova, A. Isahi, M. Najdoski, I. Grozdanov, *Mater. Res. Bull.,* 2001, **36,** 161-170.

5. J. Yin, Y. Li, F. Lv, M. Lu, K. Sun, W. Wang, L. Wang, F. Cheng, P. Xi, *Adv. Mater.,* 2017, **29,** 1704681.

6. W. Jianghao, L. Liping, L. Jing, M. Lingshen, X. Chenglin, L. Guangshe, *Chemcatchem*, 2018, **10**, 4888-4893.

7. C. Liao, Y. Zuo, Z. Wei, J. Zhao, B. Tang, A. Tang, Y. Sun, J. Xu, *Russ. J. Electrochem.,* 2013, **49,** 983-986.

8. R. R. Salunkhe, J. Tang, Y. Kamachi, T. Nakato, J. H. Kim, Y. Yamauchi, *ACS Nano,* 2015, **9,** 6288-6296.

9. P. Wen, Z. Li, P. Gong, J. Sun, J. Wang, S. Yang, *Rsc Adv.,* 2016, **6,** 13264-13271.

10. F. Meng, Z. Fang, Z. Li, W. Xu, M. Wang, Y. Liu, J. Zhang, W. Wang, D. Zhao, X. Guo, *J. Mater. Chem. A,* 2013, **1,** 7235-7241.

11. W. Meng, C. Wei, Z. Lei, H. Yang, M. Zhu, H. Yan, Y. Fu, F. Geng, Y. Jie, X. Chen, *Nano Energy,* 2014, **8,** 133-140.

12. D. Zhang, H. Shi, R. Zhang, Z. Zhang, N. Wang, J. Li, B. Yuan, H. Bai, J. Zhang, *Rsc Adv.,* 2015, **5,** 58772-58776.

13. Y. Xia, B. Wang, G. Wang, H. Wang, *Rsc Adv.,* 2015, **5,** 98740-98746.

14. D. Y. Lee, S. J. Yoon, N. K. Shrestha, S. H. Lee, H. Ahn,S. H. Han, *Micropo. Mesopor. Mater.,* 2012, **153,** 163-165.

15. Y. Z. Zhang, T. Cheng, Y. Wang, W. Y. Lai, H. Pang, W. Huang, *Adv. Mater.,* 2016, **28,** 5241-5241.

16. D. Ji, H. Zhou, J. Zhang, Y. Dan, H. Yang, A. Yuan, *J. Mater. Chem. A,* 2016, **4,** 8283-8290.

17. J. W. Jeon, R. Sharma, P. Meduri, B. W. Arey, H. T. Schaef, J. L. Lutkenhaus, J. P. Lemmon, P. K. Thallapally, M. I. Nandasiri, B. P. Mcgrail, *ACS Appl. Mater. Interface,* 2014, **6,** 7214-7222.

18. S. N. Guo, Y. Zhu, Y. Y. Yan, Y. L. Min, J. C. Fan, Q. J. Xu, H. Yun, *J. Power Sources,* 2016, **316,** 176-182.

19. P. Pachfule, D. Shinde, M. Majumder, Q. Xu, *Nat. Chem.,* 2016, **8,** 718-724.

20. A. J. Amali, J. K. Sun, Q. Xu, *Chem. Commun.,* 2014, **50,** 1519-1522.